Spectral-Domain Analysis of Scattering from *E*-Plane Circuit Elements

QIU ZHANG AND TATSUO ITOH, FELLOW, IEEE

Abstract—**The spectral-domain method is used for analysis of the scattering characteristics of *E*-plane circuit components such as nontouching *E*-plane fins. The method deals with inhomogeneous algebraic equations instead of integral equations. It provides a number of attractive features. Numerical results have been compared with those reported in the literature for special cases. Several data items useful for *E*-plane configurations are included.**

I. Introduction

RECENTLY, finlines [1], [2] and other *E*-plane structures [3]–[5] have found wide applications in millimeter-wave integrated circuits. A number of passive, active, and nonreciprocal components have been developed with the *E*-plane technique. One of the key elements for passive *E*-plane components is the *E*-plane strip. A comprehensive design process of *E*-plane bandpass filters has been reported [6]. The analysis of the *E*-plane fin connecting the top and bottom walls is relatively straightforward [6], because the problem is a two-dimensional one. On the other hand, no extensive and accurate characterizations of nontouched *E*-plane fins seem to exist. A method based on a variational technique has been introduced for a special case where there is no dielectric substrate inserted in a waveguide [7]. The method in [7] is useful for a narrow strip, because only one current component along the *E*-plane direction is used and the assumed current distribution is constant in the axial (Z) direction.

This paper introduces a new analytical technique to characterize the scattering phenomena of a number of planar *E*-plane obstacles. For instance, it can handle a wide nontouching *E*-plane fin on a dielectric substrate. Unlike the method based on the variational technique, scattering coefficients of the dominant, as well as higher order, modes can be derived. The incident mode can be either dominant or a higher order.

The method in this paper is an extension of the spectral-domain method commonly used for characterizations of eigenmodes in a printed transmission line. It is extended to the excitation problem and hence provides a set of algebraic equations corresponding to coupled integral equations that would be derived in the space domain. Compared to the integral equation method, the new technique has a number of advantages. For instance, algebraic equations are easier to handle numerically. Also, the spectral-domain Green's functions have simple closed-form expressions. Compared to the variational method [7], the present method is not only more versatile but is also attractive from a computational point of view. In the new method, it is necessary to calculate the eigenvalue of only the particular scattered mode of interest. The variational method requires evaluations of all eigenvalues. Furthermore, the method in [7] assumes that only the TE modes are scattered. By the nature of the formulation, the present method contains both TE and TM modes in its formulation.

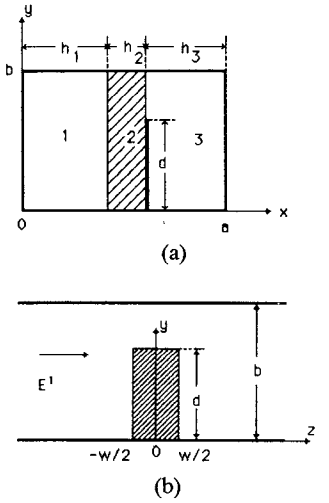

Fig. 1. *E*-plane strip in a rectangular waveguide. (a) End view. (b) Side view.

The calculated results for a special case ($\epsilon_1 = \epsilon_2 = \epsilon_3 = 1$) are compared with experimental and computed data in [7] to check the accuracy. Several curves of normalized input admittance and equivalent circuit element values are presented for a number of different parameters of the structure.

II. Formulation

In this paper, only the unilateral *E*-plane fin is treated. An application to a bilateral configuration is straightforward.

With reference to Fig. 1, the strip is assumed to be perfectly conducting and infinitesimally thin. For a given incident field E^i, the field scattered by the strip can be expressed by modal expansion. For instance, the E_y com-

Manuscript received June 12, 1986; revised September 6, 1986. This work was supported in part by the U.S. Army Research Office under Contract DAAG-29-84-K-0076.

The authors are with the Department of Electrical and Computer Engineering, University of Texas, Austin, TX 78712.

IEEE Log Number 8611630.

0018-9480/87/0200-0138$01.00 ©1987 IEEE

ponent is

$$E_y^S(x,y,z) = E_{y\,\mathrm{LSE}}^S + E_{y\,\mathrm{LSM}}^S$$

$$= \begin{cases} \sum_{m=1}^{\infty}\sum_{n=0}^{\infty} C_{mn}^{-}\phi_m(x)\cos(\alpha_n y)\,e^{j\beta_{mn}(z+W/2)}, & z<-W/2 \\ \sum_{m=1}^{\infty}\sum_{n=0}^{\infty} \phi_m(x)\cos(\alpha_n y)\left(E_{mn}^{-}e^{j\beta_{mn}z}+E_{mn}^{+}e^{-j\beta_{mn}z}\right), & |z|<W/2 \\ \sum_{m=1}^{\infty}\sum_{n=0}^{\infty} C_{mn}^{+}\phi_m(x)\cos(\alpha_n y)\,e^{-j\beta_{mn}(z-W/2)}, & z>W/2 \end{cases}$$

$$+ \begin{cases} \sum_{m=1}^{\infty}\sum_{n=1}^{\infty} D_{mn}^{-}\psi_m(x)\sin(\alpha_n y)\,e^{j\beta'_{mn}(z+W/2)}, & z<-W/2 \\ \sum_{m=1}^{\infty}\sum_{n=1}^{\infty} \psi_m(x)\sin(\alpha_n y)\left(F_{mn}^{-}e^{j\beta'_{mn}z}+F_{mn}^{+}e^{-j\beta'_{mn}z}\right), & |z|<W/2 \\ \sum_{m=1}^{\infty}\sum_{n=1}^{\infty} D_{mn}^{+}\psi_m(x)\sin(\alpha_n y)\,e^{-j\beta'_{mn}(z-w/2)}, & z>W/2 \end{cases} \tag{1}$$

where

$$\phi_m(x) = \begin{cases} C_m\sinh(\gamma_{1m}x), & 0<x<h_1 \\ A_m\sinh\left[\gamma_{2m}(x-h_1)\right]+B_m\cosh\left[\gamma_{2m}(x-h_1)\right], & h_1<x<h_1+h_2 \\ \sinh\left[\gamma_{3m}(a-x)\right], & h_1+h_2<x<a \end{cases} \tag{2}$$

$$\psi_m(x) = \begin{cases} C'_m\cosh(\gamma'_{1m}x), & 0<x<h_1 \\ A'_m\sinh\left[\gamma'_{2m}(x-h_1)\right]+B'_m\cosh\left[\gamma'_{2m}(x-h_1)\right], & h_1<x<h_1+h_2 \\ \cosh\left[\gamma'_{3m}(a-x)\right], & h_1+h_2<x<a \end{cases} \tag{3}$$

$$\alpha_n = \frac{n\pi}{b} \tag{4}$$

$$\alpha_n^2+\beta_{mn}^2 = k_i^2+\gamma_{im}^2 \tag{5a}$$

$$\alpha_n^2+\beta_{mn}'^2 = k_i^2+\gamma_{im}'^2 \tag{5b}$$

$$k_i = \omega\sqrt{\epsilon_0\mu_0\epsilon_i}, \qquad i=1,2,3. \tag{6}$$

Here, ϵ_i is the relative dielectric constant; γ_{im} and γ'_{im} are the mth eigenmodes of the LSE and LSM modes in the partially filled waveguide in region i, and they can be obtained by solving the eigenvalue equations [8]. Similar equations can be written for E_z. On the other hand, the scattered fields E_y^S and E_z^S can be expressed as follows, if the induced current components $J_y(y,z)$ and $J_z(y,z)$ are provided:

$$E_y^S(x,y,z) = \int_0^b dy'\int_{-\infty}^{\infty} dz'\left[Gyy(x,y-y',z-z')J_y(y',z')+G_{yz}(x,y-y',z-z')J_z(y',z')\right] \tag{7a}$$

$$E_z^S(x,y,z) = \int_0^b dy'\int_{-\infty}^{\infty} dz'\left[G_{zy}(x,y-y',z-z')J_y(y',z')+G_{zz}(x,y-y',z-z')J_z(y',z')\right]. \tag{7b}$$

One way to find J_y and J_z is by applying the integral equations which require the total tangential electric-field components to be zero on the strip

$$E_y^i(x,y,z)+E_y^S(x,y,z) = 0 \tag{8a}$$

$$E_z^i(x,y,z)+E_z^S(x,y,z) = 0 \qquad (x=h_1+h_2,\ y,z \text{ on strip}). \tag{8b}$$

The integral equations are

$$E_y^i(h_1+h_2,y,z)+\int_0^b dy'\int_{-W/2}^{W/2} dz'\left[G_{yy}(h_1+h_2,y-y',z-z')J_y(y',z')+G_{yz}(h_1+h_2,y-y',z-z')J_z(y',z')\right]=0 \qquad \left(0<y<b,|z|<\frac{W}{2}\right) \tag{9a}$$

$$E_z^i(h_1+h_2,y,z)+\int_0^b dy'\int_{-W/2}^{W/2} dz'\left[G_{zy}(h_1+h_2,y-y',z-z')J_y(y',z)+G_{zz}(h_1+h_2,y-y',z-z')J_z(y',z')\right]=0 \qquad \left(0<y<b,|z|<\frac{W}{2}\right). \tag{9b}$$

If those equations are solved, J_y and J_z can be obtained. These J_y and J_z are then substituted into (7), so that E_y^S and E_z^S are available everywhere. If the scattered field coefficient of a particular mode is needed, the E_y^S and E_z^S can be used in (1). Each coefficient may be found from orthogonality of the expansion functions.

Although the bove formulation is correct, we do not follow such an approach. Instead, we adopt a corresponding procedure in the Fourier-transformed domain. There are two reasons for using this new technique.

1) In the Fourier-transformed (spectral) domain, we deal with coupled algebraic equations instead of the coupled integral equations (9a) and (9b).

2) Derivations of the Green's functions in the space domain are very complicated. In the spectral domain, the Fourier-transformed Green's functions are given in closed form.

Let us introduce the Fourier transform as

$$\tilde{F}(\alpha_n,\beta)=\int_{-b}^{b} e^{j\alpha_n y}\,dy\int_{-\infty}^{\infty} f(y,z)e^{j\beta z}\,dz$$
$$\alpha_n=\frac{n\pi}{b}. \tag{10}$$

The Fourier transform of (1) at $x=h_1+h_2$ is given by

$$\tilde{E}_y^S(\alpha_n,\beta)=\tilde{E}_{y\mathrm{LSE}}^S+\tilde{E}_{y\mathrm{LSM}}^S=\sum_{m=1}^{\infty} b\delta_n\sinh(\gamma_{3m}h_3)\left\{C_{mn}^-\left[\frac{e^{-jW\beta/2}}{j(\beta+\beta_{mn})}-\pi\delta(\beta+\beta_{mn})e^{j\beta_{mn}W/2}\right]\right.$$
$$\left.+\left[E_{mn}^-\frac{\sin\frac{(\beta+\beta_{mn})W}{2}}{(\beta+\beta_{mn})}+E_{mn}^+\frac{\sin\frac{(\beta-\beta_{mn})W}{2}}{(\beta-\beta_{mn})}\right]+C_{mn}^+\left[\pi\delta(\beta-\beta_{mn})e^{j\beta_{mn}W/2}-\frac{e^{j\beta W/2}}{j(\beta-\beta_{mn})}\right]\right\}$$
$$+\sum_{m=1}^{\infty} k_n jb\cosh(\gamma'_{3m}h_3)\left\{D_{mn}^-\left[\frac{e^{-j\beta W/2}}{j(\beta+\beta'_{mn})}-\pi\delta(\beta+\beta'_{mn})e^{j\beta'_{mn}W/2}\right]\right.$$
$$+\left[F_{mn}^-\frac{\sin\frac{(\beta+\beta'_{mn})W}{2}}{\beta+\beta'_{mn}}+F_{mn}^+\frac{\sin\frac{(\beta-\beta'_{mn})W}{2}}{\beta-\beta'_{mn}}\right]$$
$$\left.+D_{mn}^+\left[\pi\delta(\beta-\beta'_{mn})e^{j\beta'_{mn}W/2}-\frac{e^{j\beta W/2}}{j(\beta-\beta'_{mn})}\right]\right\} \qquad n=0,1,2,\cdots \tag{11}$$

where

$$\delta_n=\begin{cases}2 & n=0\\ 1 & n\neq 0\end{cases} \tag{12a}$$

$$k_n=\begin{cases}1 & n\neq 0\\ 0 & n=0.\end{cases} \tag{12b}$$

The Fourier transform of (9) at $x=h_1+h_2$ is given by

$$\tilde{E}_y^i(\alpha_n,\beta)+\tilde{E}_y^S(\alpha_n,\beta)=\tilde{E}_y^t(\alpha_n,\beta) \tag{13a}$$

$$\tilde{E}_z^i(\alpha_n,\beta)+\tilde{E}_z^S(\alpha_n,\beta)=\tilde{E}_z^t(\alpha_n,\beta) \tag{13b}$$

where

$$\tilde{E}_y^S(\alpha_n,\beta)=\tilde{G}_{yy}(\alpha_n,\beta)\tilde{J}_y(\alpha_n,\beta)+\tilde{G}_{yz}(\alpha_n,\beta)\tilde{J}_z(\alpha_n,\beta) \tag{14a}$$

$$\tilde{E}_z^S(\alpha_n,\beta)=\tilde{G}_{zy}(\alpha_n,\beta)\tilde{J}_y(\alpha_n,\beta)+\tilde{G}_{zz}(\alpha_n,\beta)\tilde{J}_z(\alpha_n,\beta) \tag{14b}$$

are the scattered electric fields in the spectral domain. $\tilde{G}_{yy}$, $\tilde{G}_{yz}$, and $\tilde{G}_{zz}$ can be obtained by the immittance approach [9] (see Appendix). Notice that the right sides of (13) are not zero. This is because the application of the Fourier

transform requires the use of fields not only on the strip but also the one outside. Hence, (13) contains four unknowns, $\tilde{J}_y$, $\tilde{J}_z$, $\tilde{E}_y$, and $\tilde{E}_z$. In the process of solution by Galerkin's method, $\tilde{E}_y$ and $\tilde{E}_z$ are eliminated. To this end, let us expand $\tilde{J}_y$ and $\tilde{J}_z$ as follows:

$$\tilde{J}_y(\alpha_n,\beta)=\sum_{i=1}^{I} a_i\tilde{J}_{yi}(\alpha_n,\beta) \tag{15a}$$

$$\tilde{J}_z(\alpha_n,\beta)=\sum_{j=1}^{J} b_j\tilde{J}_{zj}(\alpha_n,\beta). \tag{15b}$$

We substitute (15) into (13) and take the inner product of the resultant equations with basis functions. Use of the Parseval's relation eliminates $\tilde{E}_y^t$ and $\tilde{E}_z^t$. The inner products of $\tilde{E}_y^t$ and $\tilde{J}_{yi}$ and of $\tilde{E}_z^t$ and $\tilde{J}_{zj}$ are zero, because $\tilde{J}_{yi}$ and $\tilde{J}_{zj}$ are Fourier transforms of the functions nonzero on the strip while $\tilde{E}_y^t$ and $\tilde{E}_z^t$ are transforms of the functions nonzero outside the strip.

The results are

$$\sum_{i=1}^{I} K_{pi}^{yy}a_i+\sum_{j=1}^{J} K_{pj}^{yz}b_j=-S_{yp},\qquad p=1,2,\cdots I \tag{16a}$$

$$\sum_{i=1}^{I} K_{qi}^{zy}a_i+\sum_{j=1}^{J} K_{qj}^{zz}b_j=-S_{zq},\qquad q=1,2,\cdots J \tag{16b}$$

where

$$K_{pi}^{yy}=\sum_{n=-\infty}^{\infty}\int_{-\infty}^{\infty}\tilde{J}_{yp}^{*}(\alpha_n,\beta)\tilde{G}_{yy}(\alpha_n,\beta)\tilde{J}_{yi}(\alpha_n,\beta)\,d\beta \tag{17a}$$

$$K_{pj}^{yz}=K_{qi}^{zy}=\sum_{n=-\infty}^{\infty}\int_{-\infty}^{\infty}\tilde{J}_{yp}^{*}(\alpha_n,\beta)\tilde{G}_{yz}(\alpha_n,\beta)\tilde{J}_{zj}(\alpha_n,\beta)\,d\beta \tag{17b}$$

$$K_{qj}^{zz}=\sum_{n=-\infty}^{\infty}\int_{-\infty}^{\infty}\tilde{J}_{zq}^{*}(\alpha_n,\beta)\tilde{G}_{zz}(\alpha_n,\beta)\tilde{J}_{zj}(\alpha_n,\beta)\,d\beta \tag{17c}$$

$$S_{py}=\sum_{n=-\infty}^{\infty}\int_{-\infty}^{\infty}\tilde{J}_{yp}^{*}(\alpha_n,\beta)\tilde{E}_y^{i}(\alpha_n,\beta)\,d\beta \tag{18a}$$

$$S_{qz}=\sum_{n=-\infty}^{\infty}\int_{-\infty}^{\infty}\tilde{J}_{zq}^{*}(\alpha_n,\beta)\tilde{E}_z^{i}(\alpha_n,\beta)\,d\beta \tag{18b}$$

where $*$ indicates the complex conjugate.

For a given incident field, we solve (16) and find a_i and b_j. Hence, $\tilde{J}_y$ and $\tilde{J}_z$ are now given.

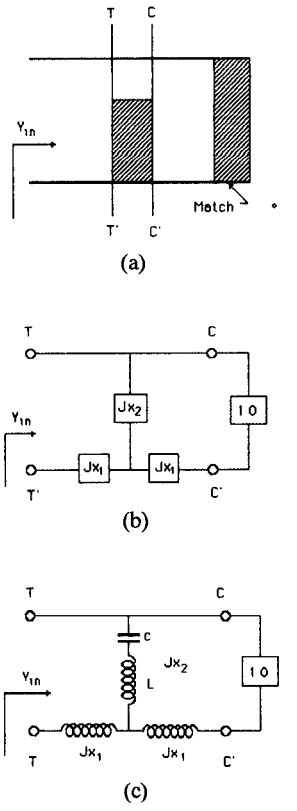

Fig. 2. (a) An E-plane strip circuit with a matched termination. (b) Two-port equivalent circuit. (c) Equivalent T-network for a narrow E-plane strip.

The scattering coefficients $C_{mn}^{\pm}$ and $D_{mn}^{\pm}$ can now be obtained. Let us express the left-hand side of (11) with (14a). Since $\tilde{G}_{yy}$ and $\tilde{G}_{yz}$ are given in closed forms and $\tilde{J}_y$ and $\tilde{J}_z$ are now known, the left-hand side of (11) is completely known. Furthermore, the left-hand side contains poles at $\beta=\pm\beta_{mn}$ and $\beta=\pm\beta'_{mn}$, since they are zeros of the denominators of $\tilde{G}_{yy}$ and $\tilde{G}_{yz}$. These values provide the eigenvalues of the LSE and LSM modes, γ_{im} and γ'_{im}. The right-hand side of (11) contains LSE poles at $-\beta_{mn}$ in the C_{mn}^{-} term and at $+\beta_{mn}$ in the C_{mn}^{+} term. It contains LSM poles at $-\beta'_{mn}$ in the D_{mn}^{-} term and at $+\beta'_{mn}$ in the D_{mn}^{+} term. Therefore, $C_{mn}^{\pm}$ and $D_{mn}^{\pm}$ can be obtained by residue calculus.

$$C_{mn}^{\pm}=\pm\lim_{\beta\to\pm\beta_{mn}}\left[(\beta\mp\beta_{mn})\frac{\tilde{G}_{yy}(\alpha_n,\beta)\tilde{J}_y(\alpha_n,\beta)+\tilde{G}_{yz}(\alpha_n,\beta)\tilde{J}_z(\alpha_n,\beta)}{jb\delta_n\sinh(\gamma_{3m}h_3)}e^{\mp jW\beta/2}\right]$$

$$\left(n=0,1,2,\cdots,m=1,2,3\cdots\delta_n=\begin{cases}2 & n=0\\ 1 & n\neq 0\end{cases}\right) \tag{19a}$$

$$D_{mn}^{\pm}=\mp\lim_{\beta\to\pm\beta'_{mn}}\left[(\beta\mp\beta'_{mn})\frac{\tilde{G}_{yy}(\alpha_n,\beta)\tilde{J}_y(\alpha_n,\beta)+\tilde{G}_{yz}(\alpha_n,\beta)\tilde{J}_z(\alpha_n,\beta)}{b\cosh(\gamma'_{3m}h_3)}e^{\mp jW\beta/2}\right]$$

$$(n=1,2,3\cdots,m=1,2,3\cdots). \tag{19b}$$

This process corresponds to the use of the orthogonality relationship to find the modal coefficients in the space domain.

TABLE I
CONFIRMATION OF POWER CONSERVATION

$d_{(mm)}$	R		T		$\|R\|^2 + \|T\|^2$
0.5	-.02008	-.02598 j	.79080	-.61119 j	1.00000
1.0	-.14712	-.13549 j	.66376	-.72071 j	1.00000
1.5	-.70508	-.10766 j	.10580	-.69288 j	1.00000
2.0	-.78485	.61825 j	.02602	.03304 j	1.00000
2.5	-.53859	.77455 j	.27229	.18934 j	1.00000
3.0	-.45482	.79016 j	.35606	.20495 j	1.00000
3.5	-.38694	.79227 j	.42394	.20705 j	1.00000

$h_1 = h_3 = 3.43$ mm; $h_2 = 0.254$ mm; $\epsilon_1 = \epsilon_3 = 1$; $b = 3.56$ mm; $w = 1.0$ m; $f = 35$ GHz; $\epsilon_2 = 2.2$.

It should be noted that in the case of E-plane fins connecting the top and bottom wall, the above equations are simplified. Since there is no field variations in the y-direction and only TE_{n0} modes are scattered for a TE_{10} excitation, we have only the one equation (13a). All the Fourier-transformed quantities are functions of β only.

III. Numerical Results

To compare the present method with the experimental and computed data in the previous publication [7], the special case $\epsilon_1 = \epsilon_2 = \epsilon_3 = 1$ is considered first. We assume that a dominant-mode incident electric field $E_{y10} = -j\beta_{10}\phi_1(x)e^{-\gamma\beta_{10}z}$, where $\phi_1(x)$ is defined in (2), comes from the left of the waveguide. The E-plane fin shown in Fig. 2(a) may be represented by an equivalent T-network, as shown in Fig. 2(b). When the waveguide is terminated with a matched load, the normalized input admittance may be represented by

$$Y_{in} = G_{in} + jB_{in} = \frac{1-R}{1+R} \tag{20}$$

where R is the reflection coefficient for the dominant mode, and can be determined in the present method by means of (19). In this study, the current basis functions are chosen as

$$J_{yi}(y,z) = \frac{\cos\left[(k-1)\left(\frac{\pi z}{W}+\frac{\pi}{2}\right)\right]}{\sqrt{1-\left(\frac{2z}{W}\right)^2}} \cdot \frac{\sin\left[(2l-1)\left(\frac{\pi y}{2d}+\frac{\pi}{2}\right)\right]}{\sqrt{1-\left(\frac{y}{d}\right)^2}} \tag{21a}$$

$$J_{zj}(y,z) = \frac{\sin\left[k\left(\frac{\pi z}{W}+\frac{\pi}{2}\right)\right]}{\sqrt{1-\left(\frac{2z}{W}\right)^2}} \frac{\cos\left[(2l-1)\left(\frac{\pi y}{2d}+\frac{\pi}{2}\right)\right]}{\sqrt{1-\left(\frac{y}{d}\right)^2}} \tag{21b}$$

where k and l are integers, and i and j are given by a combination of k and l. The equivalent circuit for a nontouching fin can be expressed as in Fig. 2(c) if the strip is not too wide. We can determine the normalized reactances X_1 and X_2 after Y_{in} in (20) is obtained. The expressions of X_1 and X_2 are given by

$$X_2 = \pm\left[\left(\frac{B_{in}}{B_{in}^2+G_{in}^2-G_{in}}\right)^2 + \frac{G_{in}-1}{B_{in}^2+G_{in}^2-G_{in}}\right]^{1/2} \tag{22a}$$

$$X_1 = \frac{B_{in}}{G_{in}-\left(B_{in}^2+G_{in}^2\right)} \mp X_2. \tag{22b}$$

The sign in (22a) and (22b) can be determined by the Foster reactance theorem in which $dx/dw > 0$ has to be satisfied for a lossless element. We can also determine the values of C and L in the equivalent circuit Fig. 2(c), once X_2 is found, under the assumption that the variations of C and L with frequency are small. The capacitance and inductance can be obtained by solving the coupled equations

$$\omega L - \frac{1}{C\omega} = X_2 \tag{23a}$$

$$L + \frac{1}{C\omega^2} = \frac{dX_2}{d\omega}. \tag{23b}$$

The numerical result has been checked by the power conservation law in which the equation $|R|^2 + |T|^2 = 1$ has to be satisfied. R and T are the reflection and transmission coefficients for the dominant mode, and can be determined from C_{10}^- and C_{10}^+ which are given by (19). The calculated results for different parameters are given in Table I. It shows that $|R|^2 + |T|^2$ is essentially 1. The convergence test with different numbers of basis functions has been performed. Although the accuracy can be increased with a larger number of basis functions, computation efforts also increase.

A comparison of the normalized susceptance versus frequency between the numerical results obtained by the present approach and those given in [7] is shown in Fig. 3(a) and (b). It is found that the numerical results agree

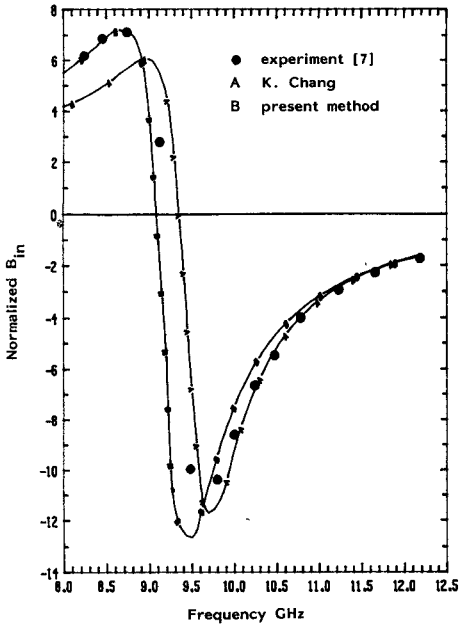

(a)

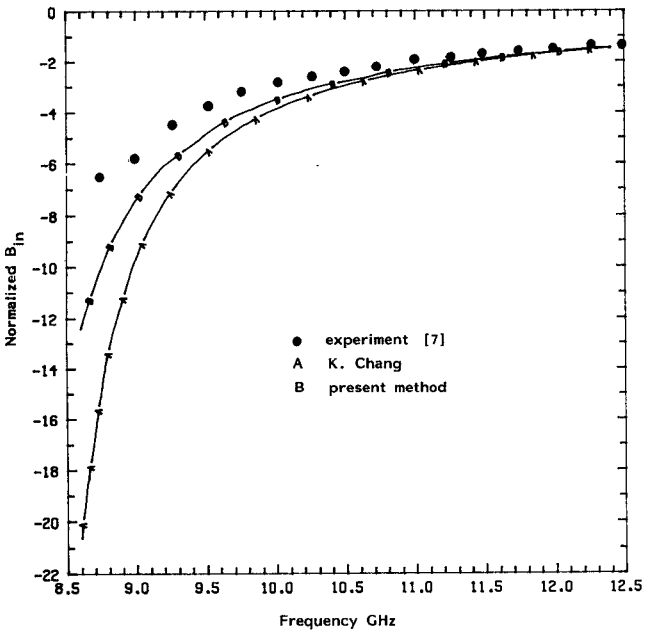

(b)

Fig. 3. Normalized susceptance of an E-plane strip in an X-band waveguide terminated with a matched load for $\epsilon_1 = \epsilon_2 = \epsilon_3 = 1$; $a = 22.86$ mm and $b = 10.16$ mm. (a) $h_1 + h_2 = 12.57$ mm, $d = 7.37$ mm, $w = 3.38$ mm. (b) $h_1 + h_2 = 11.43$ mm, $d = 9.19$ mm, $w = 1.7$ mm.

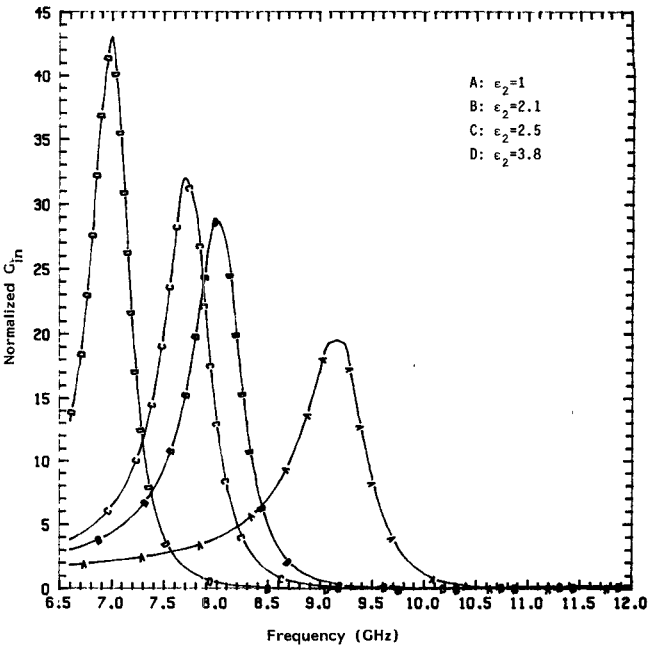

(a)

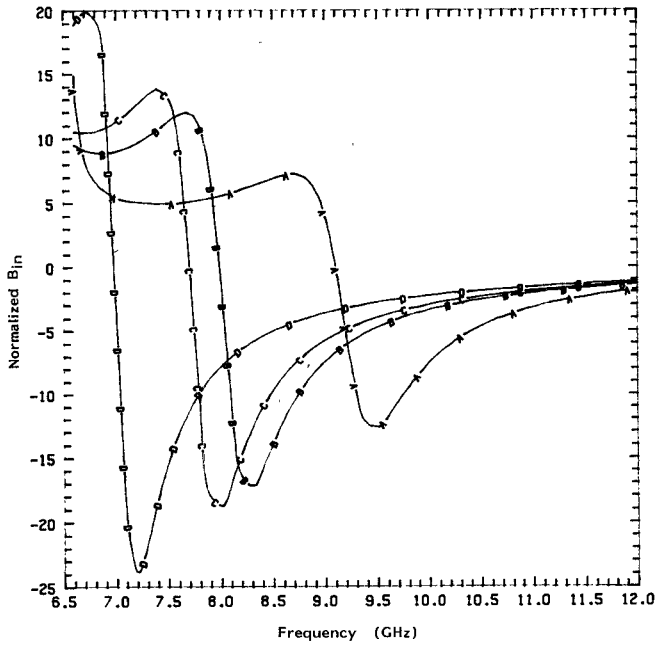

(b)

Fig. 4. Normalized admittance of an E-plane strip in an X-band waveguide terminated with a matched load versus frequency for different values of dielectric constant of the substrate. $\epsilon_1 = \epsilon_3 = 1$, $h_1 = 11.57$ mm, $h_2 = 1$ mm, $d = 7.37$ mm, and $w = 3.38$ mm. (a) Normalized conductance versus frequency. (b) Normalized susceptance versus frequency.

well with the experimental data and Chang's data. It is believed that the present method is more accurate and can be improved systematically with the use of more basis functions. Fig. 4(a) and (b) show the variations in normalized admittance versus frequency with different values of dielectric constant of the substrate in region 2. As the dielectric constant of the substrate increases, the resonant frequency at which B_{in} becomes zero decreases. This phenomenon happens because as the dielectric constant of the substrate increases, the wavelengths corresponding to each mode become shorter. The resonant frequency and the characteristics of input admittance of the considered structure can be controlled by the dielectric constant of the substrate.

Figs. 5 and 6 show the variations of normalized admittance with the height and width of the strip at different frequencies for an E-plane fin inserted in a Ka-band rectangular waveguide. Figs. 7 and 8 show the values of X_1 and X_2 versus the height d and the width w of the strip in an X-band rectangular waveguide. We note that for a

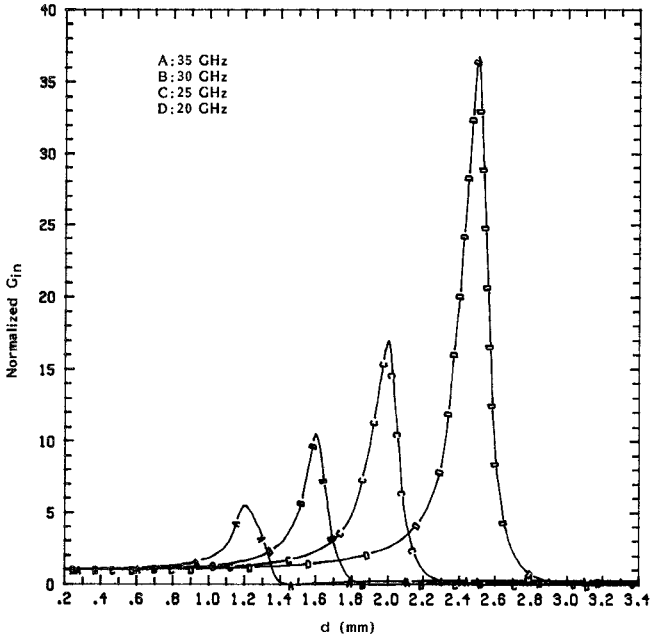

(a)

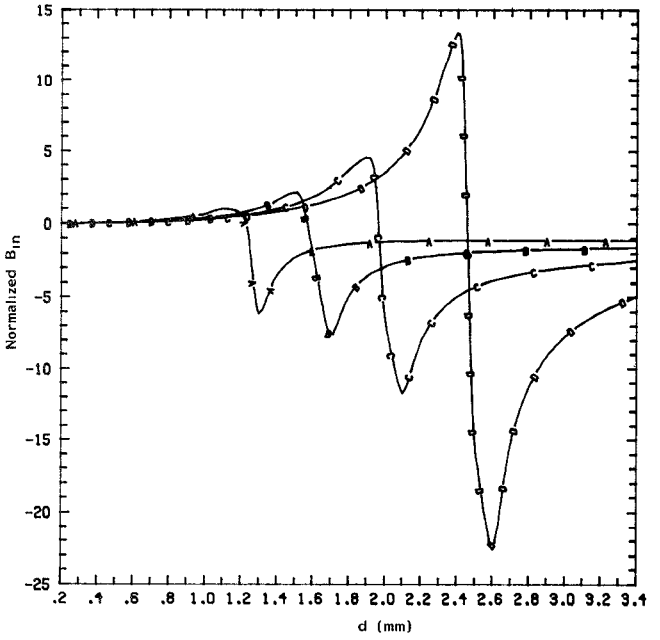

(b)

Fig. 5. Normalized admittance of an *E*-plane strip in a *Ka*-band waveguide terminated with a matched load versus strip height for different values of frequency. $\epsilon_1 = \epsilon_3 = 1$, $\epsilon_2 = 2.2$, $h_1 = 3.43$ mm, $h_2 = 0.254$ mm, $a = 7.11$ mm, $b = 3.56$ mm, $w = 1$ mm. (a) Normalized conductance versus strip height. (b) Normalized susceptance versus stri height.

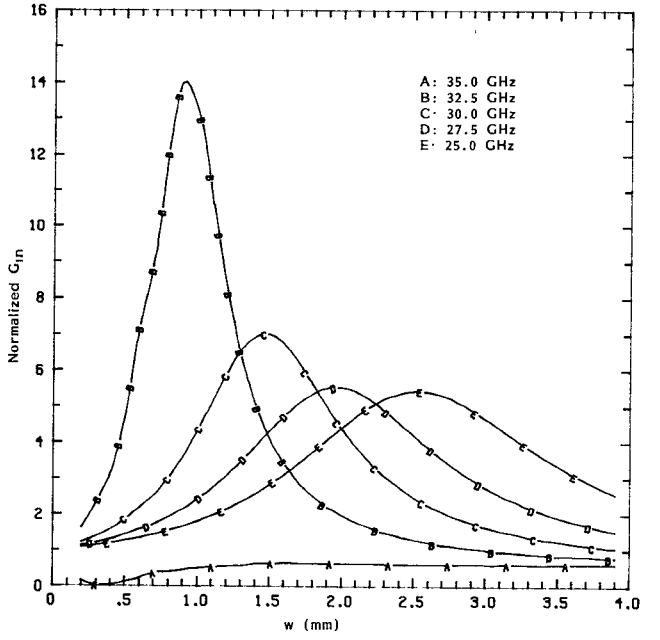

(a)

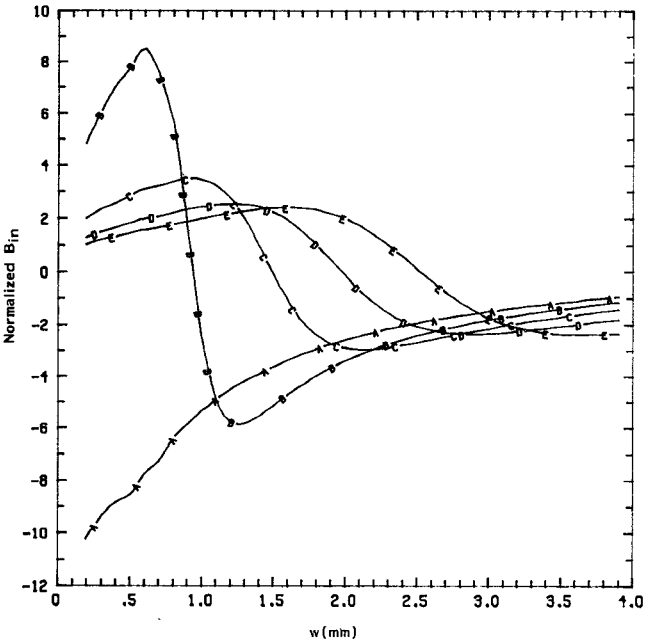

(b)

Fig. 6. Normalized admittance of an *E*-plane strip in a *Ka*-band waveguide terminated with a matched load versus strip width for different values of frequency. $\epsilon_1 = \epsilon_3 = 1$, $\epsilon_2 = 2.2$, $h_1 = 3.43$ mm, $h_2 = 0.254$ mm, and $d = 1.78$ mm. (a) Normalized conductance versus strip width. (b) Normalized susceptance versus strip width.

given frequency, X_1 is not sensitive to d whereas X_2 increases with d. When w increases, X_1 increases. On the other hand, X_2 decreases with w for a higher frequency and increases in a certain region of w for lower frequency (curve A in Fig. 8(b)). Figs. 9 and 10 are the data corresponding to those in Figs. 7 and 8 except that the frequencies are in the *Ka*-band. Figs. 11 and 12 show X_1 and X_2 versus frequency with different values of height and width for the *Ka*-band waveguide. In Fig. 12, it is seen that for a narrow strip, X_1 varies slowly as the frequency is increased, while X_2 varies faster for a narrower strip than for a wider one. Fig. 13 shows the variation of normalized capacitance C and normalized inductance L with d. We note that there are two regions. In one of them (approximately corresponding to $d > w$, in this calculation $w = 1.0$ mm) C increases and L decreases as the frequency in-

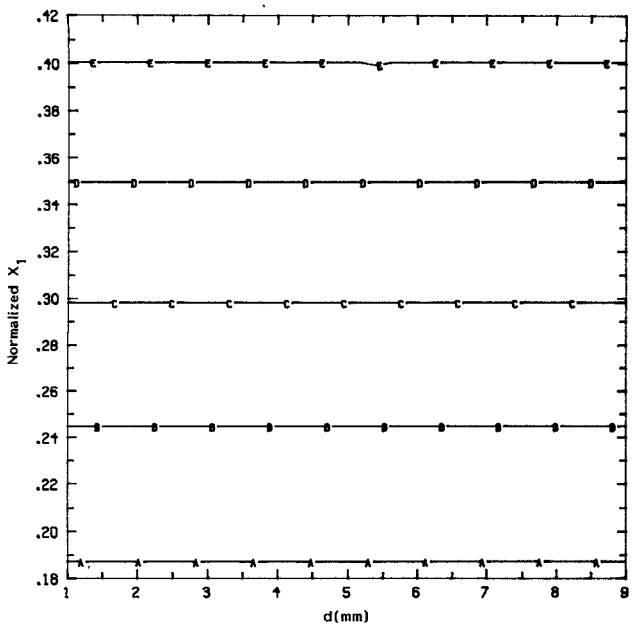

(a)

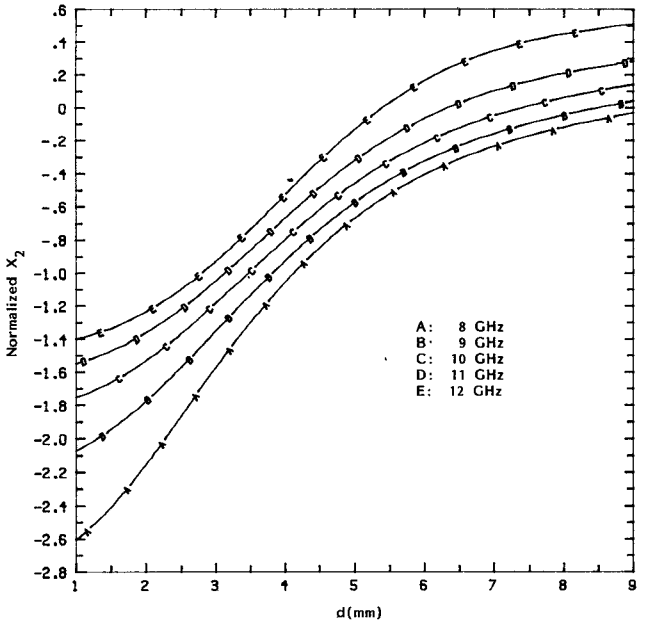

(b)

Fig. 7. Normalized reactance of equivalent circuit of an *E*-plane strip in an *X*-band waveguide versus strip height for different values of frequency. $\epsilon_1 = \epsilon_3 = 1$, $\epsilon_2 = 2.1$, $h_1 = 11.57$ mm, $h_2 = 1$ mm, and $w = 3.38$ mm. (a) Normalized X_1 versus strip height. (b) Normalized X_2 versus strip height.

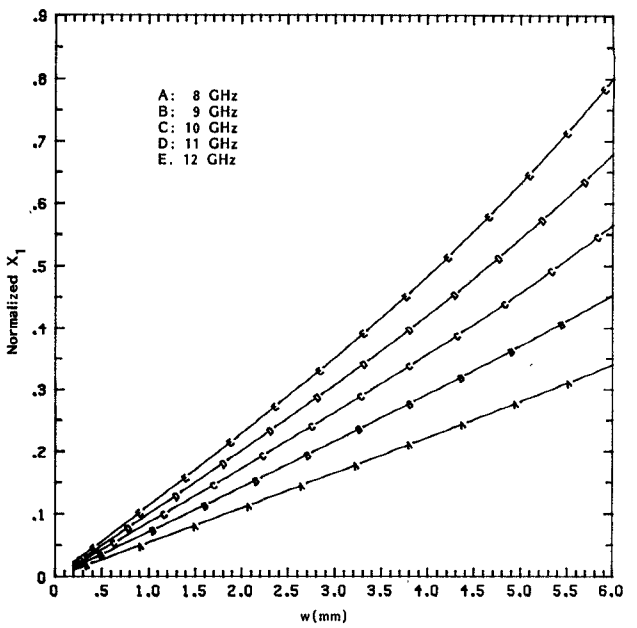

(a)

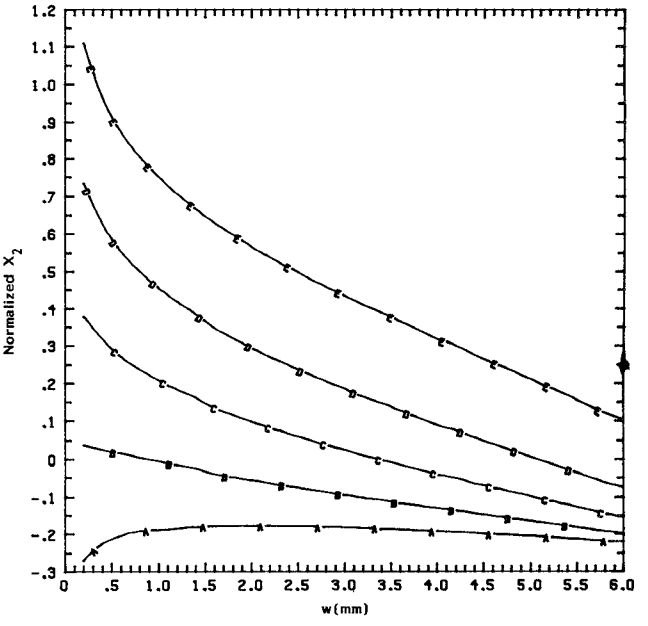

(b)

Fig. 8. Normalized reactance of equivalent circuit of an *E*-plane strip in an *X*-band waveguide versus strip width for different values of frequency. $\epsilon_1 = \epsilon_3 = 1$, $\epsilon_2 = 2.1$, $h_1 = 11.57$ mm, $h_2 = 1$ mm, and $d = 7.37$ mm. (a) Normalized X_1 versus strip width. (b) Normalized X_2 versus strip width.

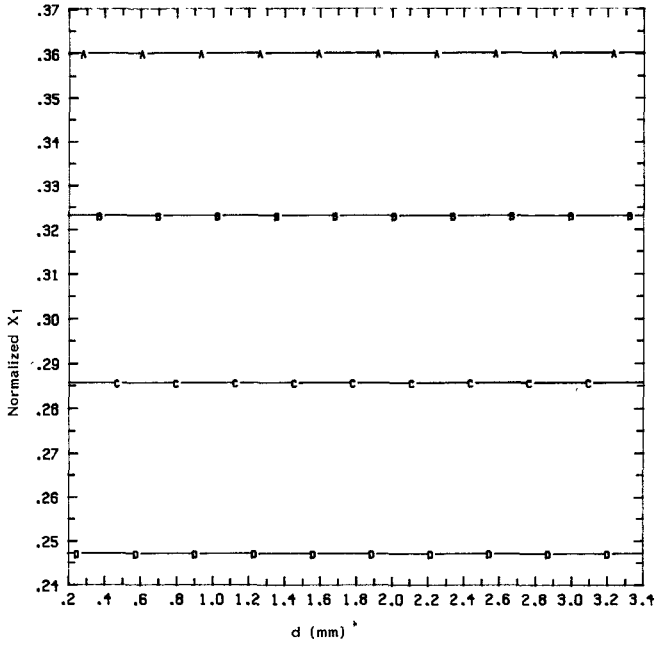

(a)

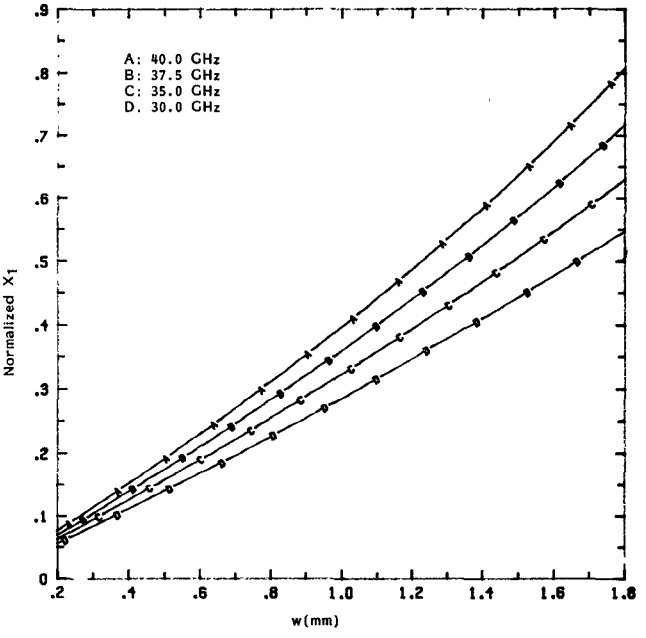

(a)

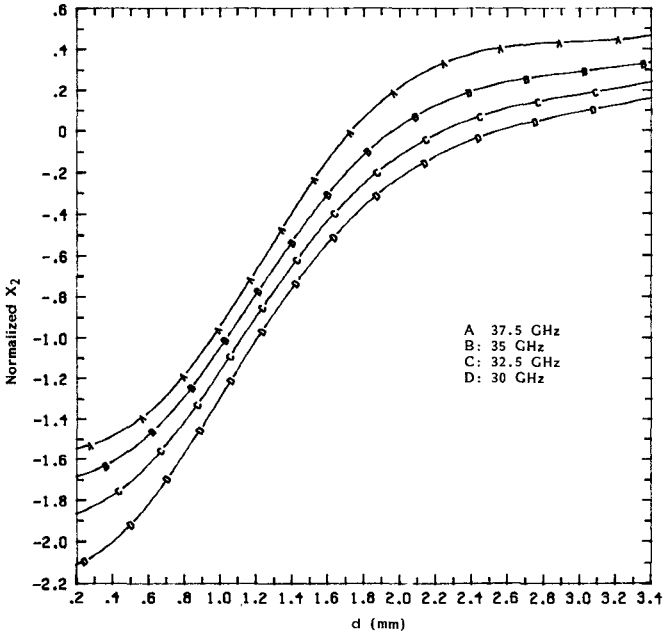

(b)

Fig. 9. Normalized reactance of equivalent circuit of an *E*-plane strip in a *Ka*-band waveguide versus strip height for different values of frequency. $\epsilon_1 = \epsilon_3 = 1$, $\epsilon_2 = 2.2$, $h_1 = 3.43$ mm, $h_2 = 0.254$ m, and $w = 1$ mm. (a) Normalized X_1 versus strip height. (b) Normalized X_2 versus strip height.

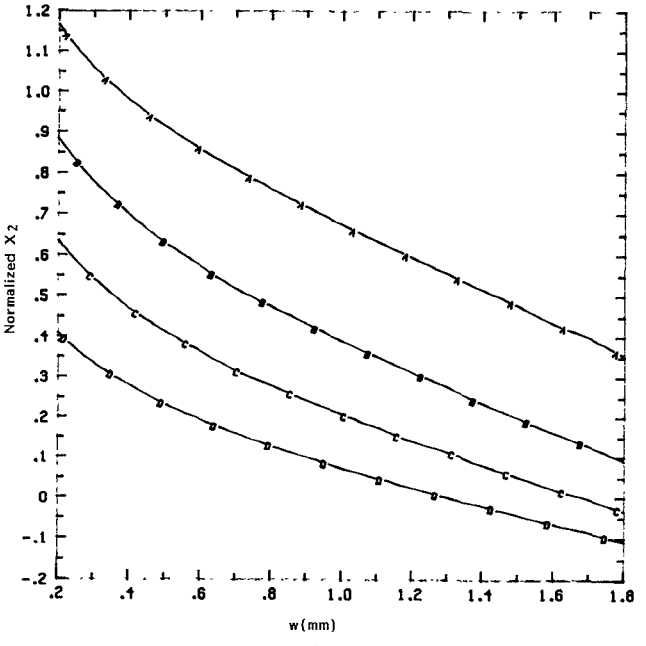

(b)

Fig. 10. Normalized reactance of equivalent circuit of an *E*-plane strip in a *Ka*-band waveguide versus strip width for different values of frequency. $\epsilon_1 = \epsilon_3 = 1$, $\epsilon_2 = 2.2$, $h_1 = 3.43$ mm, $h_2 = 0.254$ mm, and $d = 2.45$. (a) Normalized X_1 versus strip width. (b) Normalized X_2 versus strip width.

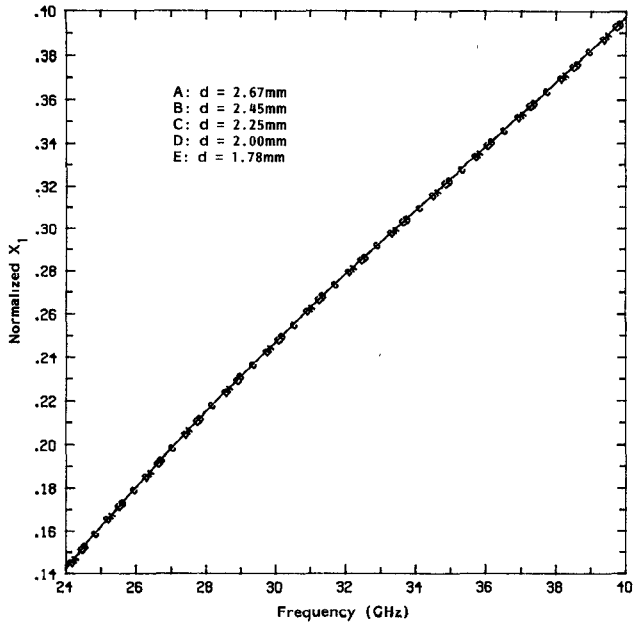

(a)

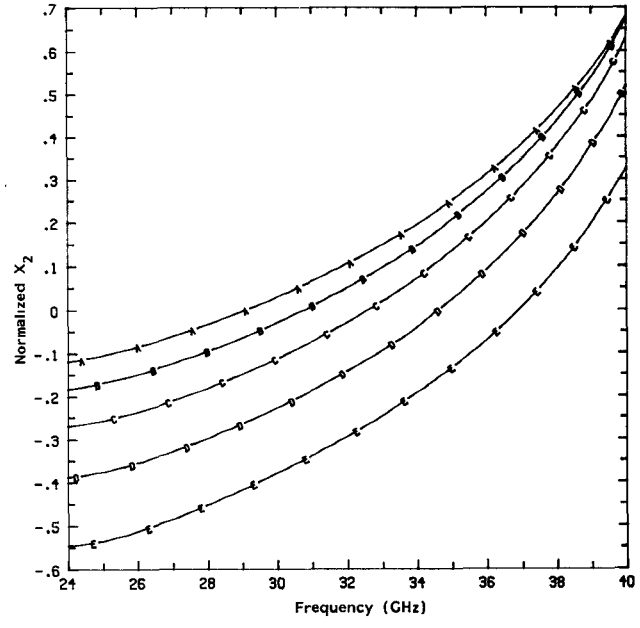

(b)

Fig. 11. Normalized reactance of equivalent circuit of an E-plane strip in a Ka-band waveguide versus frequency for different strip heights. $\epsilon_1 = \epsilon_3 = 1$, $\phi e_2 = 2.2$, $h_1 = 3.43$ mm, $h_2 = 0.254$ mm, and $w = 1$ mm. (a) Normalized X_1 versus frequency. (b) Normalized X_2 versus frequency.

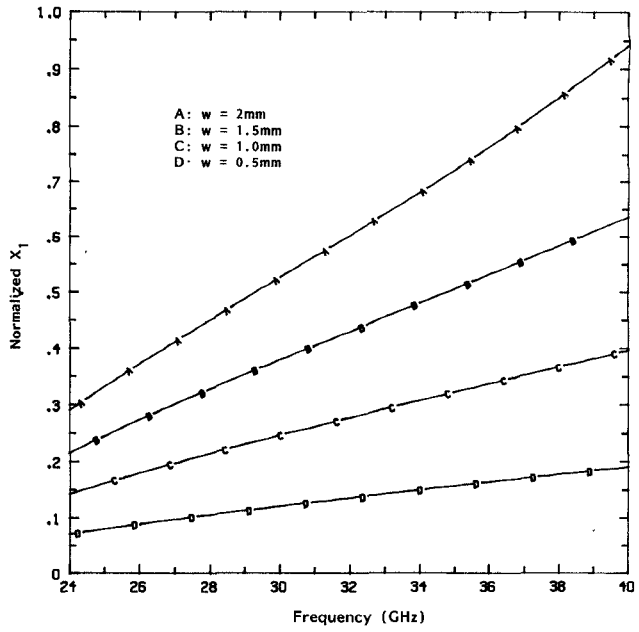

(a)

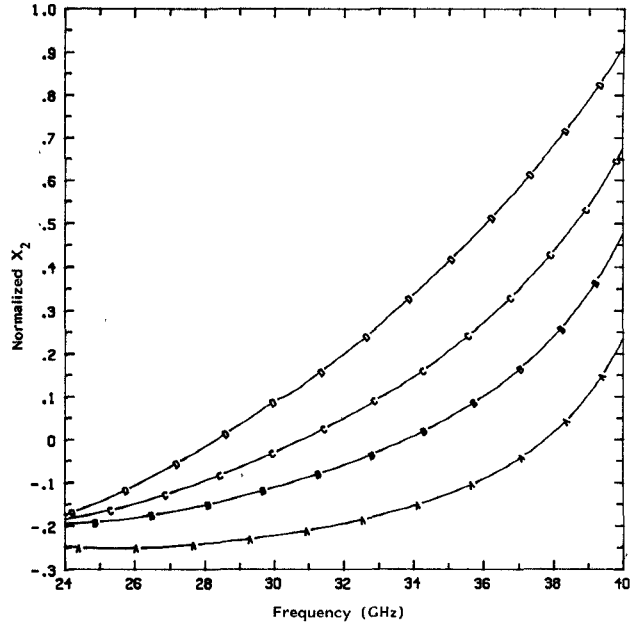

(b)

Fig. 12. Normalized reactances of equivalent circuit of an E-plane strip in a Ka-band waveguide versus frequency for different strip widths. $\epsilon_1 = \epsilon_3 = 1$, $\epsilon_2 = 2.2$, $h_1 = 3.43$ mm, $h_2 = 0.254$ mm, and $d = 2.45$ mm. (a) Normalized X_1 versus frequency. (b) Normalized X_2 versus frequency.

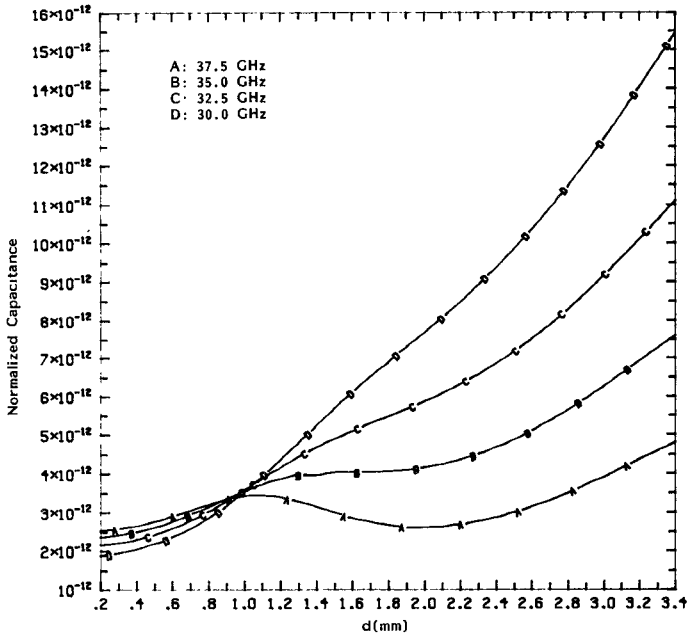

(a)

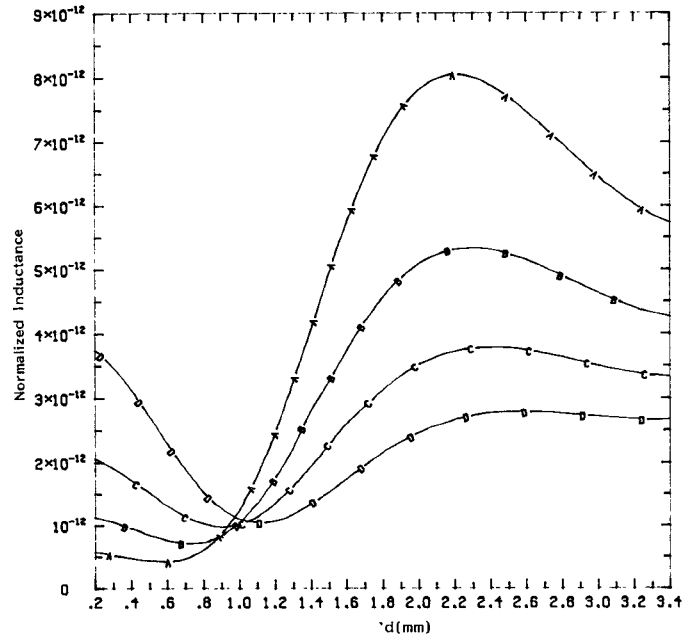

(b)

Fig. 13. Normalized equivalent circuit element values C and L of a narrow E-plane strip as a function of strip height. $\epsilon_1 = \epsilon_3 = 1$, $\epsilon_2 = 2.2$, $h_1 = 3.43$ mm, $h_2 = 0.254$ mm, and $w = 1$ mm. (a) Normalized C versus strip height. (b) Normalized L versus strip height.

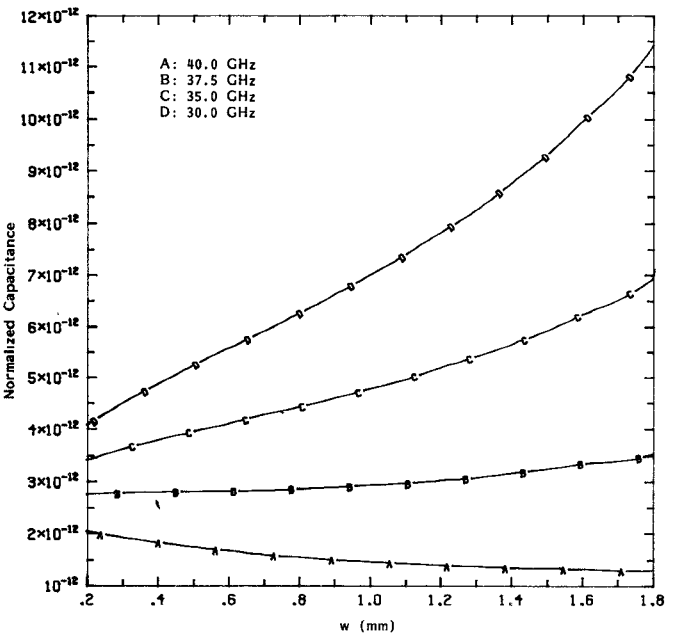

(a)

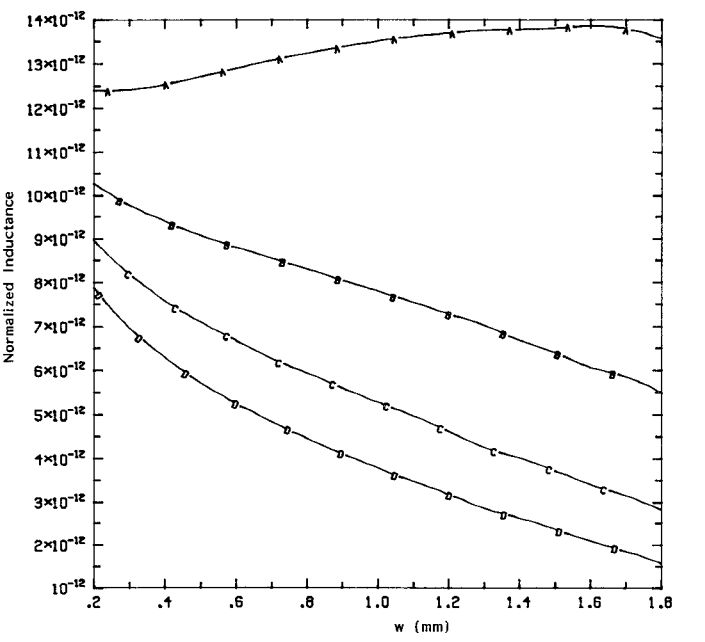

(b)

Fig. 14. Normalized equivalent circuit element values C and L of a narrow E-plane strip as a function of strip width. $\epsilon_1 = \epsilon_3 = 1$, $\epsilon_2 = 2.2$, $h_1 = 3.43$ mm, $h_2 = 0.254$ mm, and $d = 2.45$ mm. (a) Normalized C versus strip width. (b) Normalized L versus strip width.

creases. In the other region, C decreases and L increases as frequency becomes higher. It is conjectured that this phenomenon is related to the field distributions and to the use of the equivalent circuit chosen here. Fig. 14 shows the variation of C and L with w for different values of frequency.

IV. Conclusions

A new analytical technique has been developed here which can be used for characterizations of the scattering phenomena of planar E-plane obstacles. The numerical results for a special case agree well with experimental and published data. The curves of normalized input admittance and equivalent circuit element values are presented for a number of different parameters of this structure. This technique is believed to be useful in the design of microwave filters and other planar circuit components.

Appendix
Closed-Form Expression of Green's Functions in the Spectral Domain

According to [9], the TM-to-X (LSM) and TE-to-X (LSE) equivalent transmission lines for the E-plane strip described in Fig. 1 can be drawn in Fig. 15. Here,

$$\gamma_i = \sqrt{\alpha_n^2 + \beta^2 - \epsilon_i k^2} \tag{A1}$$

$$Z_{\mathrm{TM}i} = \frac{\gamma_i}{j\omega\epsilon_0\epsilon_i} \tag{A2a}$$

$$Z_{\mathrm{TE}i} = -\frac{j\omega\mu}{\gamma_i} \qquad i=1,2,3, \quad n=0,1,2,3\cdots. \tag{A2b}$$

The driving point input impedance Z^e for the TM equivalent circuit is given by

$$Z^e = \frac{1}{y_2^e + y_{2\gamma}^e} \tag{A3a}$$

where

$$y_{2\gamma}^e = y_{\mathrm{TM}3}\cdot\coth\gamma_3 h_3 \tag{A3b}$$

$$y_2^e = y_{\mathrm{TM}2}\frac{y_{\mathrm{TM}2} + y_1^e\coth\gamma_2 h_2}{y_1^e + y_{\mathrm{TM}2}\coth\gamma_2 h_2} \tag{A3c}$$

$$y_1^e = y_{\mathrm{TM}1}\coth\gamma_1 h_1. \tag{A3d}$$

Notice that y_1^e and y_2^e are input admittances looking left at $x = h_1$ and $x = h_1 + h_2$, respectively, while $y_{2\gamma}^e$ is the one looking right at $x = h_1 + h_2$. Similar equations can be written for the TE equivalent circuit

$$Z^h = \frac{1}{y_2^h + y_{2\gamma}^h} \tag{A4a}$$

$$y_{2\gamma}^h = y_{\mathrm{TE}3}\coth\gamma_3 h_3 \tag{A4b}$$

$$y_1^h = y_{\mathrm{TE}1}\coth\gamma_1 h_1 \tag{A4c}$$

$$y_2^h = y_{\mathrm{TE}2}\frac{y_{\mathrm{TE}2} + y_1^h\coth\gamma_2 h_2}{y_1^h + y_{\mathrm{TE}2}\coth\gamma_2 h_2}. \tag{A4d}$$

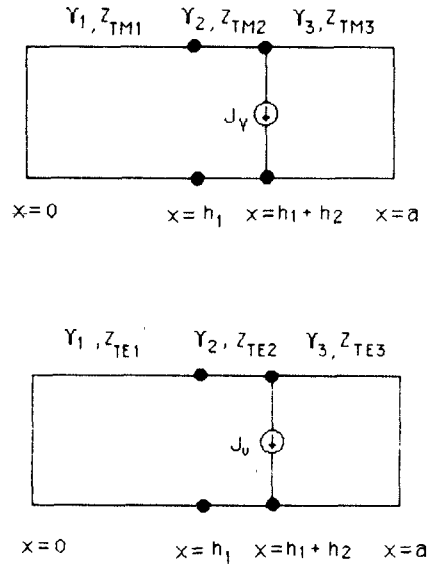

Fig. 15. The TM and TE equivalent transmission lines for the E-plant strip.

Finally, the Green's functions in the spectral domain can be represented by Z^h and Z^e as follows [8]:

$$\tilde{G}_{yy} = Z^e N_z^2 + Z^h N_y^2 \tag{A5a}$$

$$\tilde{G}_{yz} = \tilde{G}_{zy} = (Z^e - Z^h) N_z N_y \tag{A5b}$$

$$\tilde{G}_{zz} = Z^h N_z^2 + Z^e N_y^2 \tag{A5c}$$

where

$$N_z = \frac{\beta}{\sqrt{\alpha_n^2 + \beta^2}} \tag{A6a}$$

$$N_y = \frac{\alpha_n}{\sqrt{\alpha_n^2 + \beta^2}}. \tag{A6b}$$

Note that the denominators of Z^e and Z^h are the eigenvalue equations of the LSE and LSM modes.

References

[1] P. J. Meier, "Two new integrated circuit media with special advantages at millimeter wavelengths," in *IEEE-GMTT Int. Microwave Symp. Dig.*, pp. 221–223, 1972.

[2] P. J. Meier, "Integrated fin-line millimeter components," *IEEE Trans. Microwave Theory Tech.*, vol. MTT-22, pp. 1209–1216, Dec. 1974.

[3] Y. Konishi, K. Uenakada, and N. Hoshino, "The design of planar circuit mounted in waveguide and the application to low-noise 12-GHz converter," in *IEEE S-MTT Int. Microwave Symp. Dig.*, pp. 168–170, 1974.

[4] Y. Konishi and K. Uenakada, "The design of a bandpass filter with inductive strip-planar circuit mounted in waveguide," *IEEE Trans. Microwave Theory Tech.*, vol. MTT-22, pp. 869–873, Oct. 1974.

[5] Y. Konishi, "Planar circuit mounted in waveguide used as a down-converter," *IEEE Trans. Microwave Theory and Tech.*, vol. MTT-26, pp. 716–719, Oct. 1978.

[6] Y. C. Shih, T. Itoh, and L. Bui, "Computer-aided design of millimeter-wave E-plane filter," *IEEE Trans. Microwave Theory Tech.*, vol. MTT-31, pp. 135–141, Feb. 1983.

[7] K. Chang and P. J. Khan, "Equivalent circuit of a narrow axial strip in waveguide," *IEEE Trans. Microwave Theory Tech.*, vol. MTT-24, pp. 611–615, Sept. 1976.

[8] R. Collin, *Field Theory of Guided Waves*. New York: McGraw-Hill, 1960, pp. 224–232.

[9] T. Itoh, "Spectral domain immittance approach for dispersion characteristics of generalized printed transmission lines," *IEEE Trans. Microwave Theory Tech.*, vol. MTT-28, pp. 733–736, July 1980.

✠

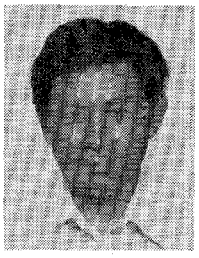

Qiu Zhang was born on October 19, 1941, in Nanchang, China. He graduated from the Jiangxi University in 1966. He received the M.S. degree in electrical engineering from the University of Texas at Austin in 1984. He is currently studying for the Ph.D. degree.

From 1967 to 1970, he was an Assistant Engineer in the Nanchang Hard Alloy Factory. In 1980 and 1981, he was employed as an engineer in the Information Institute of Science and Technology of Jiangxi province in China. His current interests are in printed-circuit components and microwave integrated circuits.

Tatsuo Itoh (S'69–M'69–SM'74–F'82) received the Ph.D. degree in electrical engineering from the University of Illinois, Urbana, in 1969.

From September 1966 to April 1976, he was with the Electrical Engineering Department, University of Illinois. From April 1976 to August 1977, he was a Senior Research Engineer in the Radio Physics Laboratory, SRI International, Menlo Park, CA. From August 1977 to June 1978, he was an Associate Professor at the University of Kentucky, Lexington. In July 1978, he joined the faculty at the University of Texas at Austin, where he is now a Professor of Electrical and Computer Engineering and Director of the Electrical Engineering Research Laboratory. During the summer of 1979, he was a guest researcher at AEG-Telefunken, Ulm, West Germany. Since September 1983, he has held the Hayden Head Centennial Professorship of Engineering at the University of Texas. Since September 1984, he has been Associate Chairman for Research and Planning of the Electrical and Computer Engineering Department.

Dr. Itoh is a member of the Institute of Electronics and Communication Engineers of Japan, Sigma Xi, and Commission B of USNC/URSI. He was Editor of the IEEE TRANSACTIONS ON MICROWAVE THEORY AND TECHNIQUES for 1983–1985, and serves on the Administrative Committee of the IEEE Microwave Theory and Techniques Society. He is a Professional Engineer registered in the state of Texas.